Infrared-to-visible upconversion in $LaCl_3$:1% Er^{3+}: Energy-level and line-strength calculations

Karl W. Krämer and Hans U. Güdel
Universität Bern, Departement für Chemie und Biochemie, Freiestrasse 3, CH 3000 Bern 9, Switzerland

Robert N. Schwartz
Hughes Research Laboratories, 3011 Malibu, California 90265-4799

(Received 28 February 1997; revised manuscript received 5 May 1997)

Single crystals of $LaCl_3$:1% Er^{3+} were grown by the Bridgman technique. Er^{3+} substitutes for La^{3+} and has a site symmetry of C_{3h} in $LaCl_3$. Seventy-three energy levels of Er^{3+} were determined up to 45 000 cm^{-1} from absorption, excitation, and luminescence spectra measured over the temperature range 4.2–293 K. A *correlated crystal-field* analysis was done by fitting 16 atomic, four crystal-field, and one correlated crystal-field parameters to the experimental Stark levels. The fit is excellent with a standard deviation of 9.0 cm^{-1}. On the basis of the wave functions thus obtained the oscillator strengths for the transitions from the $^4I_{15/2}(1)$ ground state to all the levels up to 45 000 cm^{-1} were calculated by fitting seven complex $A^{\lambda}_{t,p}$ intensity parameters to 47 observed oscillator strengths. The intensity distribution among the crystal-field components was then calculated for the inter-excited-state transition $^4I_{11/2} \rightarrow {}^4F_{7/2}$ which plays an important role in an excited-state-absorption upconversion process. [S0163-1829(97)03345-6]

I. INTRODUCTION

$LaCl_3$ is a classical host for trivalent lanthanides, and their optical spectroscopic properties have been studied in detail. Varsani and Dieke[1] reported the energy levels of f-f excited states up to 42 000 cm^{-1} more than 30 years ago. They also made attempts to reproduce the experimental energy levels with a crystal-field calculation.

It is not the purpose of the present contribution to add another paper to this series. Our work is motivated by two more recent developments. One is the search for upconversion materials for possible laser applications[2] and the other one is the development of theoretical schemes for the calculation of crystal-field levels as well as f-f intensities in lanthanide systems.[3–5]

Stimulated upconversion emission and laser action has been observed in a number of Er^{3+} doped crystals and glass fibers.[6–8] Whereas in dilute fibers upconversion clearly occurs by excited-state absorption (ESA), in bulk crystals ESA as well as energy transfer upconversion (ETU) can occur. The interplay of the two mechanisms essentially determines the upconversion behavior of a given material. We have therefore started to study these mechanisms in detail, and we have developed fingerprinting techniques for their identification, which are based on both their spectral and temporal characteristics.[9] Our effort is focused on low-phonon-energy host materials which open new upconversion luminescence pathways and suppress the detrimental multiphonon relaxation processes.[10,11]

$LaCl_3$ is an ideal host lattice in this project. $LaCl_3$ crystallizes in the hexagonal space group $P6_3/m$ with C_{3h} point symmetry for the La^{3+} site. It can easily be grown in the form of large single crystals, and is not exceedingly hygroscopic. Doping of Er^{3+} can be achieved up to a level of approximately 2%.

A crystal-field calculation on an Er^{3+} center in a C_{3h} crystal field using the formalism and programs developed by Richardson, Reid, and co-workers[3–5] can be done. Our aim is a set of high-quality wave functions which can be obtained from a fit of the model to the extensive set of absorption energies and intensities. The wave functions are then used to calculate the intensity distribution within the crystal-field multiplets for inter-excited-state transitions. Of particular interest are the potential ESA steps for upconversion, since (i) they allow an unambiguous distinction between upconversion induced by ESA and ETU and (ii) they lead to the most efficient pumping schemes for ESA upconversion. In contrast to the early work on Er^{3+} doped $LaCl_3$, therefore, we are mainly interested in the intensities obtained from the crystal-field calculation. The energy levels are used to optimize the wave functions. Since the relative intensities depend very critically on the wave functions, the highest possible quality is required.

II. EXPERIMENT

Crystals of $LaCl_3$:1% Er^{3+} were prepared from $LaCl_3$ and $ErCl_3$ which were synthesized from the oxides (Johnson & Matthey, 99.999%), NH_4Cl (Merck, p.a.) and HCl (Merck, suprapur) by the ammonium chloride route.[12] The chlorides were individually sublimed for purification in an all tantalum apparatus under vacuum. Single crystals were grown in silica ampoules by the Bridgman technique. The crystals were oriented under a polarizing microscope, embedded into epoxy resin, cut, and polished. All preparation and further handling was done in dry boxes (H_2O<1 ppm). For optical investigations the crystals were mounted in gas tight copper cells with silica windows.

Polarized absorption spectra were recorded on a Cary 5E (Varian) spectrophotometer using a closed cycle helium refrigerator (Air Products, Displex) and calcite polarizers. Polarized continuous wave upconversion luminescence spectra were obtained by argon-ion laser (Spectra Physics 2045) pumped Ti-sapphire laser (Schwartz Electrooptics) excitation

of the $^4I_{11/2}$ and $^4I_{9/2}$ states of Er^{3+}. Spectra were measured at 4.2 and 78 K using an Oxford Instruments MD 4 cryostat and at room temperature. The polarization was controlled by a polarization rotator and calcite polarizers in front and behind the sample. The luminescence passed a polarization scrambler before it entered the monochromator to prevent artifacts. The luminescence was dispersed by a 0.85 m double monochromator (Spex 1402) with gratings blazed at 500 nm (1200 grooves/mm) and detected by a cooled photomultiplier (RCA 31034) using a photon counting system (Stanford Research 400). Instrument control and data acquisition were done by a personal computer. The luminescence spectra were corrected for the wavelength dependence of the monochromator and detector sensitivity. Their ordinates were converted to units of emitted photons per unit time. The data were analyzed using the IGOR software package (Wave Metrics).

III. THEORETICAL

A. Energy-level calculations

The energy levels analyzed in this study span 22 of the 41 $^{2S+1}L_J$ multiplet manifolds of the $4f^{11}$ (Er^{3+}) electronic configuration. For these 22 manifolds, 134 crystal-field levels are predicted; however, only 73 levels are sufficiently intense, well resolved, and characterized to allow an unambiguous assignment in terms of irreducible representation and energy.

The analysis of the energy-level structure is based on the use of a parametrized effective Hamiltonian adapted to the C_{3h} site symmetry of Er^{3+} in $LaCl_3$. This semiempirical calculation utilizes matrix diagonalization and least-squares fitting techniques. The model Hamiltonian is defined to operate intraconfigurationally, i.e., entirely within the $4f^{11}$ (364 crystal-field levels) electronic configuration of Er^{3+}. In this analysis all the interactions involving $4f$-electron radial coordinates or describing intermixing from excited configurations are represented as effective parameters.

The crystal-field state vectors (expressed in an $f^{11}SLJM_J$ basis) and energies are obtained by diagonalizing the model Hamiltonian partitioned as follows:

$$\hat{\mathcal{H}}=\hat{\mathcal{H}}_A+\hat{\mathcal{H}}_{\mathrm{CF}}+\hat{\mathcal{H}}_{\mathrm{CCF}}. \tag{1}$$

Here $\hat{\mathcal{H}}_A$ represents the ''*atomic*'' Hamiltonian, which is defined to include all relevant interactions except for those that are associated with nonspherically symmetric components of the crystal-field potential, $\hat{\mathcal{H}}_{\mathrm{CF}}$ is the *one-electron* crystal-field operator, and $\hat{\mathcal{H}}_{\mathrm{CCF}}$ is the *two-electron correlation* crystal-field interaction. The explicit form of $\hat{\mathcal{H}}_A$ is given by

$$\hat{\mathcal{H}}_A=E_{\mathrm{avg}}+\alpha\hat{\mathcal{L}}(\hat{\mathcal{L}}+1)+\beta\hat{\mathcal{G}}(\hat{\mathcal{G}}_2)+\gamma\hat{\mathcal{G}}(R_7)+\sum_k F^k\hat{f}_k$$
$$+\sum_i T^i\hat{t}_i+\xi_{\mathrm{s.o.}}\hat{\mathcal{A}}_{\mathrm{s.o.}}+\sum_k P^k\hat{p}_k+\sum_j M^j\hat{m}_j, \tag{2}$$

where $k=2,4,6$, $i=2,3,4,6,7,8$, and $j=0,2,4$ and the notation used to define the various parameters and operators conforms to standard practice.[13,14]

The operator $\hat{\mathcal{H}}_{\mathrm{CF}}$, which represents the *anisotropic* components of the *one-electron* crystal-field interaction, has the following form assuming C_{3h} symmetry for the crystal-field potential at the Er^{3+} sites:

$$\hat{\mathcal{H}}_{\mathrm{CF}}=\sum_{k,q} B_q^k\hat{\mathcal{U}}_q^{(k)}=B_0^2\hat{\mathcal{U}}_0^{(2)}+B_0^4\hat{\mathcal{U}}_0^{(4)}+B_0^6\hat{\mathcal{U}}_0^{(6)}$$
$$+B_6^6[\hat{\mathcal{U}}_6^{(6)}+\hat{\mathcal{U}}_{-6}^{(6)}]. \tag{3}$$

Here $\hat{\mathcal{U}}_q^{(k)}$ are unit-tensor operators (rank k, order q) summed over all $4f$ electrons and B_q^k are parameters that contain the radially dependent parts of the one-electron crystal-field interactions and satisfy the general relationship, $B_{-q}^k=(-1)^qB_q^k$. It should be noted that the B_q^k are pure real; however, depending on the choice of the coordinate system used to define the directions perpendicular to the trigonal symmetry axis, the parameters $B_{\pm 6}^6$ can be either complex, pure real, or pure imaginary. Since the choice of the coordinate system is arbitrary, we have chosen one in which $B_{\pm 6}^6$ are pure real.

The *correlation* crystal-field operator $\hat{\mathcal{H}}_{\mathrm{CCF}}$ in Eq. (1) is formulated in terms of a set of orthogonal operators:[15–17]

$$\hat{\mathcal{H}}_{\mathrm{CCF}}=\sum_{i,K,Q} G_{iQ}^K\hat{\mathfrak{G}}_{iQ}^{(K)}, \tag{4}$$

where the number of operators varies with K, i distinguishes the different operators with identical K, K assumes even values of the integers in the range 0–12, and Q is restricted by the crystal-field symmetry. This Hamiltonian contains a large number of terms; however, previous studies have shown that only a few of these terms are needed to describe the crystal-field levels in Er^{3+} systems. For example, the $K=0$ scalar terms, which represent interelectronic Coulomb interactions, are isotropic and therefore included in $\hat{\mathcal{H}}_A$. The operators $\hat{\mathfrak{G}}_{iQ}^{(2)}$, $\hat{\mathfrak{G}}_{iQ}^{(4)}$, and $\hat{\mathfrak{G}}_{iQ}^{(6)}$ are one-electron operators and are incorporated in $\hat{\mathcal{H}}_{\mathrm{CF}}$. Even after excluding these terms there still remain 40 $G_i^K\hat{\mathfrak{G}}_i^{(K)}$ terms, each with possible multiple values of Q, depending on the local site symmetry.[17] For a more detailed discussion of the $\hat{\mathcal{H}}_{\mathrm{CCF}}$ operator the reader is referred to Refs. 15–19. Following these studies, we use here a highly restricted form of the CCF operator with only one parameter:

$$\hat{\mathcal{H}}_{\mathrm{CCF}}=G_{10A0}^4\hat{\mathfrak{G}}_{10A0}^{(4)}.$$

B. Transition line strengths

The calculation of optical line strengths for transitions between crystal-field (Stark) levels has been described in considerable detail elsewhere.[20–24] Here we only present those pertinent details that are useful for interpreting the results presented in this study. It is assumed that the observed line strengths are derived exclusively from electric- and magnetic-dipole transition mechanisms. These line strengths are calculated by evaluating

$$\mathcal{S}_{i\rightarrow f}=|\langle\Psi_i|\hat{\mu}_{\mathrm{eff}}|\Psi_f\rangle|^2+|\langle\Psi_i|\hat{m}|\Psi_f\rangle|^2, \tag{5}$$

where $\hat{\mu}_{\text{eff}}$ is an *effective* electric-dipole moment operator, $\hat{m}$ is the magnetic-dipole operator, and Ψ_i and Ψ_f are the initial and final state eigenfunctions associated with the $i \rightarrow f$ optical transition. It should be noted that the operator $\hat{\mu}_{\text{eff}}$ is defined as an even-parity operator with respect to the electronic coordinates and operates within the JM_J angular momentum basis of the $4f^{11}$ configuration. In this formulation $\hat{\mu}_{\text{eff}}$ includes the combined perturbations of the odd-parity crystal-field interactions and the odd-parity electric-dipolar radiation field interactions on the $4f$ electrons of the system. All the radial dependence of the electric-dipole transition moment is contained entirely in $\hat{\mu}_{\text{eff}}$ in parametric form.

Following previous practice,[20–24] the qth component of $\hat{\mu}_{\text{eff}}$ in a spherical basis representation is given by

$$(\hat{\mu}_{\text{eff}})_q = -e(-1)^q \sum_{\lambda,t,p,l} A^{\lambda}_{t,p} \langle \lambda l, 1-q | tp \rangle \hat{U}^{(\lambda)}_l , \qquad (6)$$

where e is the electronic charge, $\lambda = 2,4,6$; $t = \lambda, \lambda \pm 1$; $p = 0, \pm 1, \pm 2, \ldots, \pm t$ and is restricted in C_{3h} symmetry to ± 3, and $l = p + q$. The $\hat{U}^{(\lambda)}_l$ are intraconfigurational multielectron unit-tensor operators that act within the $4f^{11}$ electronic configuration, and the $A^{\lambda}_{t,p}$ are complex parameters that contain structural and mechanistic information about the interactions of the odd-parity crystal field and the electric-dipolar radiation field with the $4f$ electrons of the Er^{3+} ion.[24,25] Since the $A^{\lambda}_{t,p}$ parameters are related by the expression $(A^{\lambda}_{t,p})^* = (-1)^{t+p+l} A^{\lambda}_{t,-p}$, the total number of independent complex parameters in C_{3h} symmetry is 7: $A^2_{3,3}$, $A^4_{3,3}$, $A^4_{4,3}$, $A^4_{5,3}$, $A^6_{5,3}$, $A^6_{6,3}$, and $A^6_{7,3}$. In this study the parameters $A^{\lambda}_{t,p}$ are treated as variables in fitting the calculated line strengths to the experimental line strengths.

IV. RESULTS AND DISCUSSION

A. Crystal and point symmetry

$LaCl_3$ crystallizes in the UCl_3-type structure, which belongs to the space group $P6_3/m$ (No. 176). The unit cell consists of two formula units, with lanthanum occupying the site $(2c)$ with site symmetry 6, i.e., C_{3h} in the Schönflies notation. The La^{3+} ions are coordinated by nine Cl^- ions in the shape of a tricapped trigonal prism. In the doped crystals $LaCl_3$:1% Er^{3+}, the Er^{3+} ions randomly substitute for La^{3+} at its $(2c)$ site. No hints of clustering or the occupation of other lattice sites could be detected. The C_{3h} crystal field splits the Er^{3+} $4f^{11}$ free-ion states into Kramers doublets. For C_{3h} site symmetry the Kramers doublets transform according to the irreducible representations $(\Gamma_7 + \Gamma_8)$, $(\Gamma_9 + \Gamma_{10})$, $(\Gamma_{11} + \Gamma_{12})$,[26] which we label A, B, and C for convenience, see Table I. Also given in Table I are the selection rules for electric- and magnetic-dipole transitions. For the optical spectroscopic measurements a crystal was cut parallel to the a-c plane. Thus both $\sigma(E \perp c)$ and $\pi(E \| c)$ polarized spectra were accessible in the same experimental setup by rotating the polarizers and analyzers, when recording absorption, excitation, and luminescence spectra, respectively.

These selection rules allow an unambiguous assignment of symmetry labels to all the crystal-field levels, as will be shown below. This distinction is very important for the fit of calculated to observed energy levels.

TABLE I. Selection rules for electric- and magnetic-dipole transitions in Er^{3+} doped $LaCl_3$, site symmetry $6 = C_{3h}$. σ and π correspond to $E \perp c$ and $E \| c$, respectively. Symmetry labels: $A = \Gamma_7 + \Gamma_8 = E_{\pm 1/2}$, $B = \Gamma_9 + \Gamma_{10} = E_{\pm 5/2}$, $C = \Gamma_{11} + \Gamma_{12} = E_{\pm 3/2}$.

	A	B	C
Electric-dipole transitions			
A		σ, π	σ
B	σ, π		σ
C	σ	σ	π
Magnetic-dipole transitions			
A	σ, π		π
B		σ, π	π
C	π	π	σ

B. Energy levels

The energies of the Er^{3+} levels in $LaCl_3$:1% Er^{3+} were determined from absorption, excitation, and luminescence spectra. They are listed in the fourth column of Table II as A, E, and L, respectively. A survey absorption spectrum at 15 K in σ polarization is shown in Fig. 1. At 15 K only the lowest Stark level of the $^4I_{15/2}$ ground manifold is populated. The spectrum shows the sharp $4f^{11} \rightarrow 4f^{11}$ transitions between the ground state and the states up to 45 000 cm^{-1}. The onset of the strong parity allowed $4f^{11} \rightarrow 4f^{10}5d^1$ transition at about 41 000 cm^{-1} prohibits a measurement beyond 45 000 cm^{-1}. From the transitions to the $J = \frac{3}{2}$ states, e.g., $^4S_{3/2}$ and $^4F_{3/2}$, the symmetry label of the lowest ground-state level $^4I_{15/2}(1)$ can be determined. As shown in Fig. 2, the $^4I_{15/2}(1) \rightarrow {}^4F_{3/2}$ transition exhibits two lines. Both lines are observed in σ polarization, but only one in π polarization. Because the $^4F_{3/2}$ manifold consists of two Stark levels with A and C symmetry, respectively, it follows from Table I that the lowest ground-state level $^4I_{15/2}(1)$ must have B symmetry. Since this $^4I_{15/2}(1)$ level is the initial level of all the observed absorption transitions at cryogenic temperatures, we can use the observed polarization properties to assign symmetry labels to all the final states. This is because the three types of transitions $B \rightarrow A$, B, and C have distinct and mutually exclusive selection rules, as shown in Table I. In addition, Table I also shows that the transitions originating from a B level are either of electric- or magnetic-dipole origin; no mixtures can occur. This is illustrated in Fig. 3, which shows the $^4I_{15/2}(1) \rightarrow {}^4I_{13/2}$ polarized absorption spectra with the electric-dipole (ED) and magnetic-dipole (MD) selection rules in the inset. The MD transitions are hatched. Contributions from a magnetic-dipole mechanism are only observed for $^4I_{15/2} \rightarrow {}^4I_{13/2}$. All other lines in the absorption spectra are of ED origin and the symmetry labels of the final levels are either A or C. Because the $B \rightarrow B$ transitions are ED forbidden, the energies of the B levels were derived from luminescence and excited-state absorption spectra. This was possible up to $^4G_{11/2}$ with the exception of $^2H_{11/2}$, whose luminescence is quenched by multiphonon relaxation to $^4S_{3/2}$. Above 27 000 cm^{-1} only a few levels could be individually resolved because of the decreasing resolution of the absorption spectrometer and the low intensity of many of the transitions. The crystal-field levels of the ground state were obtained from luminescence spectra, e.g., the $^4S_{3/2} \rightarrow {}^4I_{15/2}$,

TABLE II. Electronic states, symmetry labels, experimental and calculated energy levels, and line strengths of $LaCl_3$:1% Er^{3+}. The line strengths are given for the transitions originating from $^4I_{15/2}(1)$. Values in parentheses are not used for the fitting procedure. The symmetry labels are defined in Table I. The column ''Det.'' refers to the determination of the energy levels: *A* from absorption, *E* from excitation, and *L* from luminescence spectra. Magnetic-dipole transitions are marked by *.

State	CF level	Sym. label	Det.	Energy (cm^{-1})			Line strength (10^{-8} D^2)			
				Observed	Calculated	Diff.	σ_{obs}	σ_{calc}	π_{obs}	π_{calc}
$^4I_{15/2}$	1	*B*	*L*	0	−9.9	9.9				
	2	*C*	*L*	36(1)	29.4	6.6				
	3	*C*	*L*	63(1)	57.9	5.1				
	4	*A*	*L*	95(1)	90.9	4.1				
	5	*B*	*L*	112(1)	108.1	3.9				
	6	*C*	*L*	140(1)	139.5	0.5				
	7	*A*	*L*	179(1)	177.5	1.5				
	8	*A*	*L*	228(1)	219.5	8.5				
$^4I_{13/2}$	1	*B*	*A*	6 548.3(4)	6 553.4	−5.1	(147*)		(92*)	
	2	*C*	*A*	6 564.5(4)	6 571.7	−7.2	28	29	(92*)	
	3	*A*	*A*	6 573.0(4)	6 581.0	−8.0	28	25	55	32
	4	*A*	*A*	6 586.5(4)	6 595.1	−8.6	311	303	458	538
	5	*B*	*A*	6 589.8(4)	6 596.8	−7.0	(18*)		(37*)	
	6	*C*	*A*	6 615.8(4)	6 622.9	−7.1	36	29		
	7	*A*	*A*	6 643.2(4)	6 650.8	−7.6	236	195		20
$^4I_{11/2}$	1	*B*	*E*	10 206(1)	10 202.5	3.5				
	2	*C*	*A*	10 207.6(6)	10 204.8	2.8	118	101		
	3	*A*	*A*	10 210.5(6)	10 209.4	1.1		4	83	71
	4	*B*	*E*	10 222(1)	10 219.7	2.3				
	5	*A*	*A*	10 227.4(6)	10 226.3	1.1	47	57	94	121
	6	*C*	*A*	10 240.6(6)	10 240.5	0.1	18	11		
$^4I_{9/2}$	1	*B*	*E*	12 389(1)	12 382.8	6.2				
	2	*C*	*A*	12 398.2(5)	12 387.7	10.5	39	37		
	3	*C*	*E*	12 467(1)	12 456.1	10.9		7		
	4	*A*	*A*	12 491.4(5)	12 478.9	12.5	96	88	29	32
	5	*B*	*E*	12 545(1)	12 533.2	11.8				
$^4F_{9/2}$	1	*C*	*A*	15 252.4(4)	15 267.7	−15.3	8	8		
	2	*B*	*L*	15 269(1)	15 279.7	−10.7				
	3	*A*	*A*	15 277.0(4)	15 290.7	−13.7	166	336	39	31
	4	*C*	*A*	15 303.4(4)	15 314.2	−10.8	236	253		
	5	*B*	*L*	15 315(1)	15 325.3	−10.3				
$^4S_{3/2}$	1	*C*	*A*	18 384.7(7)	18 386.2	−1.5	52	69		
	2	*A*	*A*	18 408.7(7)	18 407.9	0.8	118	171	190	301
$^2H_{11/2}$	1	*B*			19 105.0					
	2	*B*			19 138.0					
	3	*C*	*A*	19 133.3(7)	19 141.1	−7.8	233	244		
	4	*A*	*A*	19 138.8(7)	19 155.6	−16.8	107	137	170	349
	5	*C*	*A*	19 158.6(7)	19 166.4	−7.8	491	718		
	6	*A*	*A*	19 175.7(7)	19 178.4	−2.7	515	405	1823	1707
$^4F_{7/2}$	1	*B*	*L*	20 477(1)	20 472.0	5.0				
	2	*C*	*A*	20 498.4(9)	20 491.3	7.1	82	108		
	3	*B*	*L*	20 530(1)	20 525.0	5.0				
	4	*A*	*A*	20 550.6(9)	20 542.2	8.4	82	79	587	436
$^4F_{5/2}$	1	*C*	*A*	22 165(1)	22 166.5	−1.5	82	101		
	2	*B*	*L*	22 171(1)	22 164.0	7.0				
	3	*A*	*A*	22 181(1)	22 177.4	3.6	54	84	11	17
$^4F_{3/2}$	1	*C*	*A*	22 500(1)	22 498.5	1.5	43	35		
	2	*A*	*A*	22 528(1)	22 526.9	1.1	107	97	203	180
$^2H_{9/2}$	1	*B*	*L*	24 502(1)	24 512.9	−10.9				
	2	*C*	*A*	24 508(1)	24 517.5	−9.5	20	18		

TABLE II. (*Continued*).

State	CF level	Sym. label	Det.	Energy (cm^{-1}) Observed	Calculated	Diff.	Line strength (10^{-8} D^2) σ_{obs}	σ_{calc}	π_{obs}	π_{calc}
	3	*C*	*A*	24 565(1)	24 571.9	−6.9	49	37		
	4	*A*	*A*	24 599(1)	24 600.9	−1.9	64	23	15	8
	5	*B*	*L*	24 626(1)	24 632.6	−6.6				
$^4G_{11/2}$	1	*B*	*L*	26 325(1)	26 323.1	1.9				
	2	*C*	*A*	26 351(1)	26 351.4	−0.4	105	105		
	3	*B*	*L*	26 357(1)	26 348.8	8.2				
	4	*A*	*A*	26 363(1)	26 370.4	−7.4	183	178	293	409
	5	*C*	*A*	26 382(1)	26 375.2	6.8	594	1095		
	6	*A*	*A*	26 404(1)	26 394.2	9.8	744	532	3287	2170
$^4G_{9/2}$	1	*B*			27 344.1					
	2	*C*	*A*	27 358(1)	27 358.6	−0.6	(48)	134		
	3	*A*	*A*	27 364(1)	27 358.0	6.0	(79)	50	(35)	132
	4	*B*			27 359.5					
	5	*C*			27 366.9			33		
$^2K_{15/2}$	1	*A*	*A*	27 596(2)	27 595.7	0.3	(26)	2	(17)	1
	2	*C*			27 612.6			4		
	3	*B*			27 643.8					
	4	*B*			27 687.1					
	5	*C*			27 712.7			6		
	6	*A*			27 712.9			11		22
	7	*C*			27 714.4			7		
	8	*A*			27 723.1			1		2
$^4G_{7/2}$	1	*B*			27 982.8					
	2	*A*		27 987(2)	27 989.5	−2.5	(319)	87	(142)	58
	3	*B*			27 989.7					
	4	*C*			27 993.6			109		
$^2P_{3/2}$	1	*C*	*A*	31 468(1)	31 466.1	1.9	(8)	6		
	2	*A*	*A*	31 506(1)	31 501.7	4.3	(11)	14	(34)	32
$^2K_{13/2}$	1	*A*			32 844.1			3		3
	2	*C*			32 856.6			2		
	3	*B*			32 870.8					
	4	*B*			32 906.8					
	5	*A*			32 925.9			2		2
	6	*C*			32 943.2			2		
	7	*A*			32 963.9			6		
$^2P_{1/2}$	1	*A*			33 031.9					
$^4G_{5/2}$	1	*C*			33 203.0					
	2	*B*			33 231.3					
	3	*A*			33 248.1			2		
$^4G_{7/2}$	1	*B*			33 904.9					
	2	*B*			33 936.5					
	3	*A*	*A*	33 956(2)	33 955.4	0.6	(220)	53	(202)	87
	4	*C*			33 961.2			76		
$^2D_{5/2}$	1	*B*			34 623.7					
	2	*A*			34 636.7			9		2
	3	*C*			34 651.5			11		
$^2H_{9/2}$	1	*B*			36 324.8					
	2	*C*			36 398.8			3		
	3	*A*	*A*	36 421(2)	36 404.1	16.9	(60)	29		14
	4	*B*			36 464.1					
	5	*C*			36 467.5			11		
$^4D_{5/2}$	1	*B*			38 470.7					
	2	*A*			38 471.7			16		2

TABLE II. (*Continued).*

State	CF level	Sym. label	Det.	Energy (cm^{-1}) Observed	Calculated	Diff.	Line strength (10^{-8} D^2) σ_{obs}	σ_{calc}	π_{obs}	π_{calc}
	3	*C*			38 479.6			9		
$^4D_{7/2}$	1	*A*	*A*	38 949(2)	38 943.6	5.4	(665)	1468	(829)	2778
	2	*C*	*A*	38 956(2)	38 962.2	−6.2	(594)	1902		
	3	*B*			38 975.1					
	4	*B*			39 051.4					
$^2I_{11/2}$	1	*C*	*A*	40 828(2)	40 837.3	−9.3	(44)	23		
	2	*A*	*A*	40 852(2)	40 840.3	11.7		28	(212)	130
	3	*B*			40 878.0					
	4	*C*			40 899.0			15		
	5	*A*			40 935.1			14		7
	6	*B*			40 949.3					
$^2L_{17/2}$	1	*A*	*A*	41 226(2)	41 235.7	−9.7	(64)	18	(146)	8
	2	*C*	*A*	41 263(2)	41 251.0	12.0	(41)	26		
	3	*B*			41 271.9					
	4	*B*			41 321.5					
	5	*C*			41 339.0			7		
	6	*A*			41 349.8			2		21
	7	*A*			41 353.9			39		53
	8	*C*			41 381.7			25		
	9	*B*			41 469.5					
$^4D_{3/2}$	1	*C*			42 017.7			6		
	2	*A*			42 035.5			10		18
$^2P_{3/2}$	1	*A*			42 693.2					
	2	*C*			42 715.7					
$^2I_{13/2}$	1	*A*			43 312.8			32		11
	2	*C*	*A*	43 320(2)	43 318.0	2.0	(147)	26		
	3	*B*			43 331.5					
	4	*A*	*A*	43 340(2)	43 348.7	−8.7	(89)	11		
	5	*C*			43 364.5			6		
	6	*B*			43 383.0					
	7	*A*			43 456.7			2		

see Fig. 4. The lowest level of the $^4S_{3/2}$ manifold has symmetry label *C* and thus the ED allowed transitions $C \rightarrow A$ and *B* are observed in σ polarization, and the $C \rightarrow C$ transitions in π polarization. The transitions into the higher levels of the $^4I_{15/2}$ ground state, especially $1' \rightarrow 6$ and $1' \rightarrow 7$, are significantly broadened due to coupling with phonon sidebands of the higher-energy transitions. $LaCl_3$ has Raman active phonons at 219, 212, 186, 180, and 108 cm^{-1} at 78 K.[27]

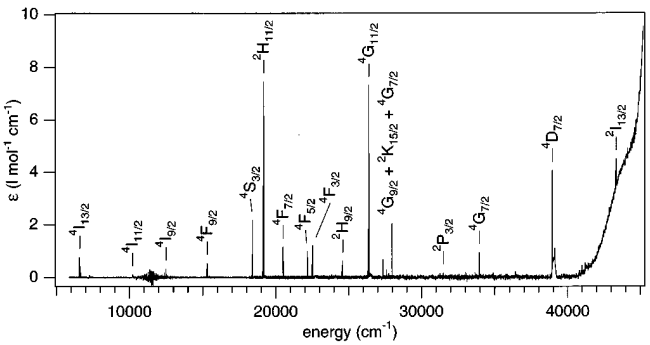

FIG. 1. Survey optical absorption spectrum of $LaCl_3$:1% Er^{3+} at 15 K in σ polarization.

The energies and symmetry labels of the levels in Table II are in agreement with earlier work.[1,4,28] The starting point for our energy calculations was the free Er^{3+} ion with $|SLJM_J\rangle$ basis functions. Initial values for the atomic and crystal-field parameters were taken from the work of Jayasankar, Reid, and Richardson.[4] The calculation was done for the full $4f^{11}$-electron configuration leading to a 364×364 energy matrix. Following Ref. 4 the *M* and *P* atomic parameters were correlated according to $M^0 = 1.78M^2 = 2.63M^4$ and $P^2 = 1.33P^4 = 2P^6$, in order to reduce the number of free parameters. The Er^{3+} site symmetry C_{3h} gives rise to four one-electron crystal-field parameters, B_0^2, B_0^4, B_0^6, and B_6^6. In the fitting procedure 16 atomic and four crystal-field parameters, as well as one CCF parameter, G^4_{10A0}, were freely varied (see Sec. III A). The standard deviation defined as

$$\sigma = \left(\frac{1}{n-p} \sum_{i=1}^{n} [\tilde{\nu}(i)_{obs} - \tilde{\nu}(i)_{calc}]^2 \right)^{1/2}, \qquad (7)$$

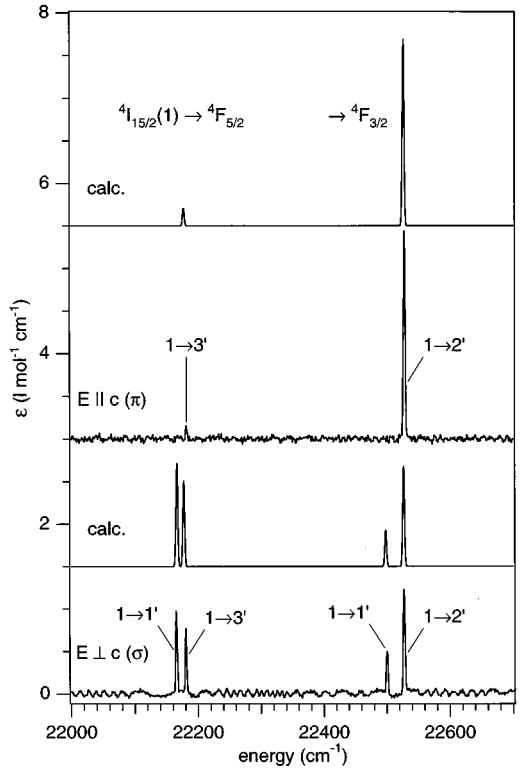

FIG. 2. Observed and calculated absorption spectra at 15 K of the $^4I_{15/2}(1) \rightarrow {}^4F_{5/2}$ and $^4F_{3/2}$ transitions in σ and π polarization. The parameter values in Tables III and IV were used for the calculation.

where n is the number of input energy levels and p the number of parameters, was used as a measure of the goodness of the fit. Inclusion of the CCF parameter resulted in a slight improvement of σ from 9.2 to 9.0 cm^{-1}. The final parameter values are listed in Table III together with their uncertainties which are calculated to be the square roots of the respective diagonal element of the error matrix multiplied by σ. The calculated energy levels are included in

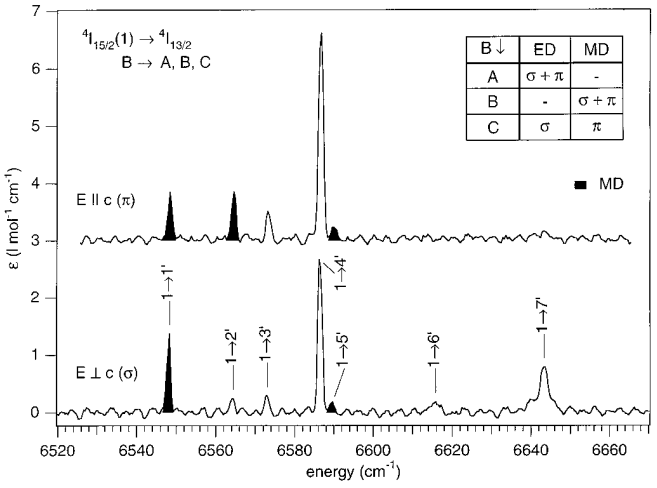

FIG. 3. Absorption spectra of the $^4I_{15/2}(1) \rightarrow {}^4I_{13/2}$ transition in σ and π polarization at 15 K. The magnetic-dipole transitions are hatched. The relevant selection rules are reported in the insert.

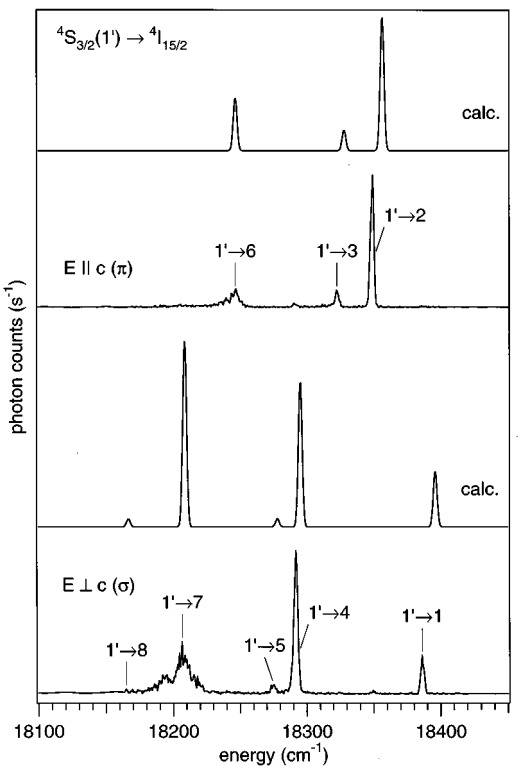

FIG. 4. Observed and calculated luminescence spectra of the $^4S_{3/2}(1') \rightarrow {}^4I_{15/2}$ transition in σ and π polarization at 4.2 K. The parameter values in Tables III and IV were used for the calculation.

Table II. For the designation of term symbols we use the convention of Varsani and Dieke,[1] even in those two cases in which our calculation yields a different major $|SLJM_J\rangle$ contribution to the wave function.

With a standard deviation of 9.0 cm^{-1} the overall agreement between experimental and calculated energies is excellent. It is better than in the recently performed analysis of Er^{3+} in $CsCdBr_3$,[29] in which Er^{3+} occupies a C_{3v} site and with a total of 65 energy levels a σ value 11.2 cm^{-1} was obtained using the same formalism as in the present paper. Similar analyses of the Er^{3+} energy-level structure in $Cs_3Lu_2Cl_9$ (Ref. 30) and $Cs_3Lu_2Br_9$,[31] again with C_{3v} site symmetry, yielded σ values of 18.0 and 19.3 cm^{-1}, respectively. We find a very modest improvement of 0.2 cm^{-1} of the least-squares fit by including the CCF parameter. In contrast, the standard deviation improved by 7.6, 4.8, and 4.6 cm^{-1} when CCF parameters were introduced in the above-mentioned three analyses, respectively. We can only speculate as to why a straightforward analysis using only one-electron crystal-field terms yields a significantly better agreement in the case of $LaCl_3$ than $CsCdBr_3$, $Cs_3Lu_2Cl_9$, and $Cs_3Lu_2Br_9$ host lattices. The C_{3h} point symmetry leads to the mutually exclusive selection rules in Table I and eventually to an unambiguous symmetry labeling of all the determined energy levels. In C_{3v} there are only two possible symmetry labels instead of three and the assignment is not as unambiguous. In addition, C_{3v} is an approximation for $Cs_3Lu_2Cl_9$ and $Cs_3Lu_2Br_9$, the actual exact point group being C_3. This might be a possible source for the higher standard deviation. Another possibility is the difference in the actual coordination. In the quoted C_{3v} examples the coordination is

TABLE III. Atomic, crystal-field, and correlated crystal-field parameter values of $LaCl_3$:1% Er^{3+} (in cm^{-1} units). The parameters are defined in Sec. III A. The values were obtained from fitting 21 parameters to 73 experimental data resulting in an overall standard deviation of $\sigma = 9.0\ cm^{-1}$.

	Parameter		
E_{avg}	35 459	±	12
F^2	98 260	±	45
F^4	69 793	±	62
F^6	48 114	±	71
ζ	2 362	±	3
α	17.4	±	1.7
β	−638	±	10
γ	2 061	±	38
T^2	426	±	19
T^3	48	±	5
T^4	22	±	7
T^6	−305	±	13
T^7	289	±	17
T^8	353	±	18
M^0	4.2	±	1.4
P^2	416	±	20
B_{20}	−248	±	16
B_{40}	−303	±	20
B_{60}	529	±	16
B_{66}	−351	±	13
G^4_{10A0}	194	±	31

a trigonally distorted octahedron, whereas in the $LaCl_3$ host it is a tricapped trigonal prism with a mirror plane perpendicular to the threefold axis. It is conceivable that the simple model is sufficient to fully account for this situation but not the distorted octahedron. The significant improvement of the fit upon inclusion of a CCF term in all these studies possibly results from a deficiency of the simple model, and it may have nothing to do with a correlated crystal-field interaction.

Let us finally compare our analysis with the results of two previous studies of Er^{3+} doped $LaCl_3$ which both use the experimental data of Varsani and Dieke.[1] Most parameters reported in Table III coincide within their standard deviation with those reported by Jayasankar, Reid, and Richardson.[4] They used the same parametrization scheme as in our work except the CCF parameter. Their fit of 20 parameters to 83 energy levels resulted in a standard deviation of $\sigma = 10.5\ cm^{-1}$. We find slightly smaller values for the Slater integrals F^4 (−0.4%) and F^6 (−3%). More serious discrepancies occur for γ, T^2, and T^7 for which they report values of 1787(35), 286(21), and 172(19) cm^{-1}, respectively. If we take our values in the context of those of the whole lanthanide series[4] our γ and T^7 values are reasonable. Our γ is equal to that reported for Ho^{3+} and their value of T^7 seems to be extraordinarily small. Our $T^2 = 426\ cm^{-1}$ may be overestimated and a value around 300 cm^{-1} more reasonable. Besides the calculations of Jayasankar, Reid, and Richardson[4] there exists a remarkable early work of Eisenstein[28] where a D_{3h} symmetry of Er^{3+} is assumed instead of C_{3h}. An excellent standard deviation of 3.8 cm^{-1} is archived for 72 energy levels by varying eight parameters (F^2, F^4, F^6, ζ, and four crystal-field parameters) in a root-mean-square fit plus a linear approximation scheme. However, this calculation is not directly comparable to our present work due to the different mathematics.

Inspecting Table II reveals that the atomic parameters contribute more to the standard deviation than the crystal-field parameters. For example, the $^4I_{13/2}$ multiplet as a whole has a deviation of $-7.2\ cm^{-1}$, but the deviations within the multiplet remain within the range -2.1–$1.4\ cm^{-1}$. This indicates that the atomic part rather than the crystal-field part should be worked on to improve the overall fit.

C. Line strengths

The calculation of line strengths serves two purposes. First it is a very rigorous test of the wave functions obtained in the energy calculation. If we are able to reproduce the measured intensities, our confidence in the quality of the energy calculation will be strengthened. The second reason is more important. We have the possibility to calculate inter-exited-state transitions which are not or not easily accessible by experiment, but which are potentially important for excited-state-absorption processes or stimulated emission in a potential laser.

Experimental line strengths $S_{i\to f}$ of the $4f\to 4f$ transitions originating from the $^4I_{15/2}(1)$ level were determined from the 15 K absorption spectra. The spectra were recorded in ϵ (l/mol cm) versus $\tilde{\nu}$ (cm^{-1}) units. The line strengths in squared Debye units (D^2) were then obtained by using the following equation:

$$S = \frac{3h\epsilon_0 c\ \ln 10}{2\pi^2 N_L \chi_{ed} \tilde{\nu}} \int \epsilon(\tilde{\nu}) d\tilde{\nu} = \frac{9.186\,45\times 10^{-3}}{\chi_{ed}\tilde{\nu}} \int \epsilon(\tilde{\nu}) d\tilde{\nu}, \tag{8}$$

where

$$\chi_{ed} = (n^2+2)^2/9n \tag{9}$$

is the correction factor for bulk refractivity $\chi_{ed}(LaCl_3) = 1.7645$ for $n = 1.849$ and the remaining symbols have their usual meaning. The integration is over the absorption line profile.

Because all crystal-field levels in $LaCl_3$:Er^{3+} are Kramers doublets each line consists of four transitions which are pairwise degenerate. The sum over the four transitions yields the line strength reported in Table II. The lines observed in the absorption spectra are of electric-dipole origin only, except for some lines within the $^4I_{15/2}\to{}^4I_{13/2}$ manifold which are of magnetic-dipole origin, see Fig. 3. No MD lines were detected in the luminescence and excitation spectra. The intensity calculations were therefore only done for the electric-dipole transitions.

In the fitting procedure the quantity $[(I_{obs}-I_{calc})/(I_{obs}+I_{calc})]^2$ is minimized where I_{obs} and I_{calc} are the observed and calculated line strengths, respectively. As a measure of the quality of the fit a dimensionless standard deviation is calculated,

$$\sigma = \left[\frac{1}{n-p}\sum_{i=1}^{n}\left(\frac{I_{obs}-I_{calc}}{I_{obs}+I_{calc}}\right)^2\right]^{1/2}, \tag{10}$$

TABLE IV. $A^{\lambda}_{t,p}$ intensity parameter values of $LaCl_3$:1% Er^{3+}. The complex numbers are given as $(\mathbf{a}+i\mathbf{b})$ in units of 10^{-13} cm. The parameters are defined in Sec. III B. Left-hand side: 14 parameters were fitted to 47 experimental data resulting in an overall standard deviation of $\sigma=0.20$. Right-hand side. For comparison a fit without the $A^4_{4,3}$ and $A^6_{6,3}$ parameters is reported, see Sec. IV C, which yields $\sigma=0.30$ for 47 experimental data and ten intensity parameters. The uncertainties of the parameter values are the square roots of the respective diagonal elements of the error matrix multiplied by σ.

	a	b	a	b
$A^2_{3,3}$	−126±8	547±12	−537±13	215±5
$A^4_{3,3}$	−901±9	−199±4	−991±8	525±3
$A^4_{4,3}$	152±9	−484±3		
$A^4_{5,3}$	179±7	569±4	78±4	186±3
$A^6_{5,3}$	−50±5	226±2	146±3	174±5
$A^6_{6,3}$	46±3	403±2		
$A^6_{7,3}$	347±3	37±3	512±2	−11±2

where n is the number of data points and p the number of variables. Forty-seven experimentally determined line strengths were used to determine seven complex $A^{\lambda}_{t,p}$ parameters, see Sec. III B, which were decomposed as $(\mathbf{a}+i\mathbf{b})$ resulting in 14 variables. This fit results in a standard deviation of $\sigma=0.20$ which represents an uncertainty factor $(1+\sigma)/(1-\sigma)=1.5$ for the quantity $I_{\rm obs}/I_{\rm calc}$. The final parameter values are given in Table IV.

A comparison of experimental and calculated absorption intensities is given in Table II in numerical form and for the selected transitions $^4I_{15/2}(1)\rightarrow{}^4F_{5/2}$ and $^4F_{3/2}$ in Fig. 2 in graphical form. For the calculation of the spectra a Gaussian line shape is used with a full width at half maximum (FWHM) of 3.33 $\rm cm^{-1}$ which corresponds to that of the measured spectra. The energies of the calculated spectra in Fig. 2 are taken from the sixth column of Table II: calculated energies. The calculated line strengths are transformed to an ϵ representation according to Eq. (8).

In analogy to absorption transitions we can calculate the intensity distribution of luminescence transitions. This calculation is based on the $A^{\lambda}_{t,p}$ parameters determined from the experimental absorption intensities. In order to get the correct value for spontaneous emission we have to multiply the line strengths $S_{i\rightarrow f}$ from Eq. (5) by a factor $\tilde{\nu}^3$.[32] Since the experimental luminescence intensities are not on an absolute scale, they are scaled to the calculated values for a given multiplet. Figure 4 compares the calculated and measured spectra for the $^4S_{3/2}(1')\rightarrow{}^4I_{15/2}$ multiplet.

The agreement between calculated and experimental intensity distributions is excellent in both Figs. 2 and 4 for both polarizations. The degree of agreement shown here is typical for the other transitions, see also Table II. This confirms the validity of our theoretical approach and the high quality of the wave functions obtained with the model parameters in Tables III and IV. To our knowledge we present such extensive intensity calculations for the individual crystal-field components of Er^{3+} in both absorption and emission for the first time. No attempt was made in the earlier work on Er^{3+} doped $LaCl_3$ to compute individual line strengths.

The $A^{\lambda}_{t,p}$ parameters can provide information about the mechanism of the spectroscopic transitions.[20,21] The $A^{\lambda}_{t,p}$ parametrization scheme implies a one-photon-one-electron process. In the work of Burdick *et al.*[33] it was used to test the validity of the assumption that each M-L interacts independently with the radiation field. In this case the $A^{\lambda}_{t,p}$ parameters with $\lambda=t$ are expected to vanish, and this was found to be the case in YAG:Nd^{3+} (YAG denotes yttrium aluminum garnet).[33] In contrast, we find that for $LaCl_3$:Er^{3+} all seven $A^{\lambda}_{t,p}$ parameters are needed for a good reproduction of the intensities. A calculation setting $A^4_{4,3}$ and $A^6_{6,3}$ equal to zero and fitting the remaining parameters to the experimental line strengths resulted in a significantly inferior fit with $\sigma=0.30$. The result of this fit is included in Table IV. We conclude that the so-called superposition model is not a good approximation for $LaCl_3$:Er^{3+}.

The average of the squares of the $A^{\lambda}_{t,p}$ parameters can be used as a measure of the average f-f transition intensity of a material. Unfortunately, no comparable line-strength study of an Er^{3+} system is available. We can compare with two studies on other rare earth ions, i.e., YAG:Nd^{3+} (Ref. 33) and $Na_3[M(oda)_3]\cdot 2NaClO_4\cdot 6H_2O$ (which we abbreviate as oda) with $M=Nd^{3+}$, Sm^{3+}, Eu^{3+}, and Ho^{3+}.[34] The average of the squared $A^{\lambda}_{t,p}$ parameters of $LaCl_3$:Er^{3+} is about 5–10 times smaller than for (oda) systems and 50 times smaller than for YAG:Nd^{3+}. It is difficult to interpret these differences with the available narrow data base. Relevant factors may be the position of the first $4f\rightarrow 5d$ excitation for a given lanthanide ion, the degree of covalency in the metal-ligand bond, the charge of the ligand, and the coordination geometry. A systematic variation of only one of these parameters will be necessary to determine its influence on the overall f-f intensity.

D. Upconversion

Based on the results presented above we can now use the same procedures and results to predict the intensity distribution for transitions which are not directly observable but play an important part in upconversion processes. One process of importance in near-infrared–to–visible upconversion of Er^{3+} involves a $^4I_{15/2}\rightarrow{}^4I_{11/2}$ excitation in a first step and a $^4I_{11/2}\rightarrow{}^4F_{7/2}$ excited-state absorption in a second step. We have experimentally identified this process as important in $LaCl_3$:Er^{3+} and recorded the resulting $^4F_{7/2}\rightarrow{}^4I_{15/2}$ luminescence. The results of this extensive work will be published separately. Here we demonstrate the importance and significance of being able to compute the intensity distribution for both steps in the ESA upconversion. The upper two traces of Fig. 5 show the calculated spectra for both the $^4I_{15/2}\rightarrow{}^4I_{11/2}$ and the $^4I_{11/2}\rightarrow{}^4F_{7/2}$ steps. The intensity distribution was obtained for 78 K by assuming a Boltzmann population among the crystal-field levels in the initial state for both steps. In contrast to Figs. 2 and 4 the experimental CF energies were used. The bottom trace of Fig. 5 shows an experimental upconversion excitation spectrum at 78 K.

Figure 5 is very instructive. The two excitation multiplets $^4I_{15/2}\rightarrow{}^4I_{11/2}$ and $^4I_{11/2}\rightarrow{}^4F_{7/2}$ are displaced with only a very small overlap at 10 239 $\rm cm^{-1}$ at 78 K. The two crystal-field transitions $^4I_{15/2}(1)\rightarrow{}^4I_{11/2}(6)$ (first step) and $^4I_{11/2}(6)\rightarrow{}^4F_{7/2}(1)$ (second step) have a mismatch of only

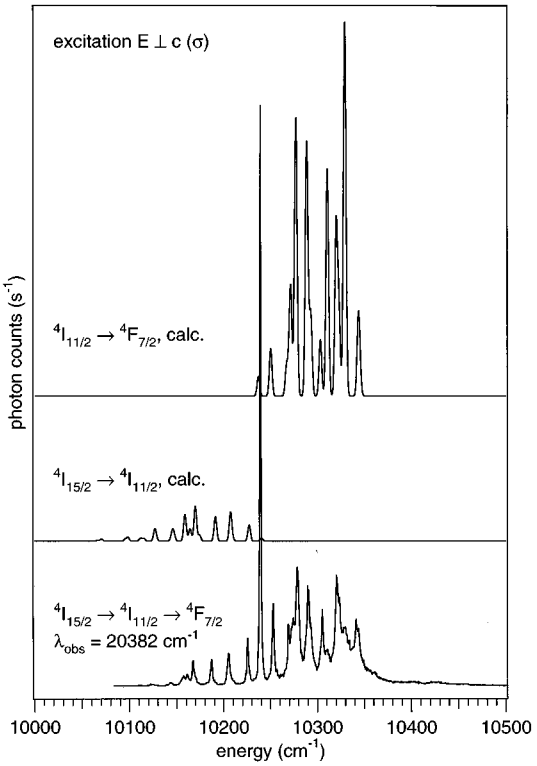

FIG. 5. Upper two traces: Calculated intensity distributions for the $^4I_{11/2} \rightarrow {}^4F_{7/2}$ and $^4I_{15/2} \rightarrow {}^4I_{11/2}$ excitations at 78 K assuming a Boltzmann distribution in the initial state. The parameter values in Tables III and IV were used. Lowest trace: Experimental upconversion excitation spectrum monitoring the $^4F_{7/2}(1') \rightarrow {}^4I_{15/2}(4)$ luminescence (20 382 cm^{-1}) at 78 K. The spectrum is not corrected for the decrease in laser intensity towards lower energies.

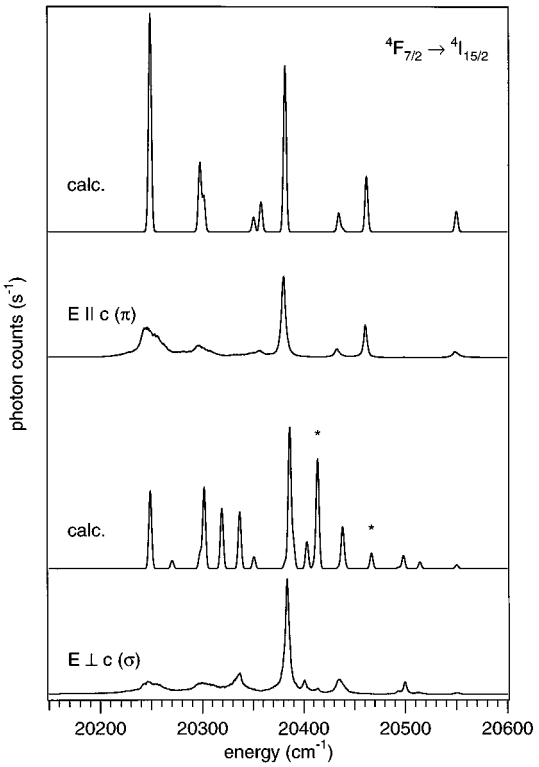

FIG. 6. Observed and calculated luminescence spectra of the $^4F_{7/2} \rightarrow {}^4I_{15/2}$ transition at 78 K in σ and π polarization. The parameter values in Tables III and IV were used for the calculation. The $^4F_{7/2} \rightarrow {}^4I_{15/2}(3)$ transitions are marked by asterisks.

3 cm^{-1} around this energy, see Table II. The temperature of 78 K was chosen because the intermediate $^4I_{11/2}(6)$ level has almost no population at 4.2 K. On the other hand, at 295 K there is substantial overlap of the excitation lines due to line broadening, and individual transitions can hardly be recognized. The experimental upconversion excitation spectrum has the most prominent line at 10 239 cm^{-1}. Weaker excitation lines occur on both the high- and low-energy side of the 10 239 cm^{-1} line, and Fig. 5 shows very convincingly that they correspond to $^4I_{15/2} \rightarrow {}^4I_{11/2}$ and $^4I_{11/2} \rightarrow {}^4F_{7/2}$ CF excitations, respectively. All the lines below 10 239 cm^{-1} are due to $^4I_{15/2} \rightarrow {}^4I_{11/2}$ CF excitations in the first step followed by transitions from vibronic levels of $^4I_{11/2}$ to CF levels of $^4F_{7/2}$ in the second step. Above 10 239 cm^{-1} the first excitation step consists of vibronic $^4I_{15/2} \rightarrow {}^4I_{11/2}$ transitions followed by electronic $^4I_{11/2} \rightarrow {}^4F_{7/2}$ CF excitations. Time-resolved experiments show a simple exponential decay without rise for all the excitation lines at 78 K, which confirms the ESA mechanism of the upconversion process. The high intensity of the 10 239 cm^{-1} excitation line shows the importance of resonance. Despite the mismatch of 3 cm^{-1} there is some overlap of the two electronic lines. Figure 5 also shows that for both steps the two lines are very weak compared to other components of the $^4I_{15/2} \rightarrow {}^4I_{11/2}$ and $^4I_{11/2} \rightarrow {}^4F_{7/2}$ multiplets, respectively. Thus the actual overlap of intensity for the two absorption steps at 10 239 cm^{-1} is very small, and yet this line stands out in the experimental excitation spectrum. This immediately suggests a two-color excitation scheme in which the two energies are matched to the most intense CF components for the two steps. According to Fig. 5 two orders of magnitude in excitation efficiency should be gained in such a process. Our first experiments confirm these expectations.

Calculated and measured $^4F_{7/2} \rightarrow {}^4I_{15/2}$ upconversion luminescence spectra at 78 K are shown in Fig. 6. As for Fig. 5 a Boltzmann population among the CF levels is assumed and the experimental CF energies are used for the calculation. For the line shape calculation again a Gaussian with FWHM of 3.33 cm^{-1} is used which is adequate for the lines above 20 370 cm^{-1}. The lines below 20 370 cm^{-1} are strongly broadened due to coupling with phonon sidebands of the higher-energy transitions. This line broadening is generally observed for transitions to the higher-energy CF levels, see also Figs. 3 and 4. The agreement between the calculated and experimental intensity distribution shown in Fig. 6 is very good, with the exception of the $^4F_{7/2} \rightarrow {}^4I_{15/2}(3)$ intensities which are overestimated by the calculation in σ polarization; the respective lines are marked by asterisks. It is worth noting here that $^4F_{7/2}$ luminescence is not observed in oxides and fluorides and only very rarely in chlorides, but it is prominent in most bromides and iodides upon $^4I_{11/2}$ excitation. $^4F_{7/2} \rightarrow {}^2H_{11/2}$ multiphonon relaxation is very competitive in the host lattices with higher phonon energies. In this respect $LaCl_3$:Er^{3+} has a bromidelike behavior, and a substantial $^4F_{7/2}$ population relaxes radiatively by luminescence around 20 400 cm^{-1}.

In conclusion we can say that the $LaCl_3:Er^{3+}$ system studied here appears to be ideally suited for a crystal-field calculation of the highest quality. This may have to do with the C_{3h} point symmetry and the tricapped trigonal prismatic coordination. The excellent agreement between experimental and calculated energies and line strengths demonstrates the essential correctness of the chosen parametrization scheme. The high quality of the wave functions and parameters obtained allows the calculation of intensity distributions for processes which are not directly accessible by experiment, but which are of high relevance for an understanding of upconversion and possibly cross-relaxation processes. We have chosen the example of a $^4I_{15/2} \rightarrow {}^4I_{11/2} \rightarrow {}^4F_{7/2}$ ESA upconversion process to demonstrate the potential of the technique. There are many other processes which determine steady-state populations in a cw excitation experiment or excited-state dynamics in a pulsed experiment. A good set of wave functions and parameters will be a very powerful tool, in addition to the experimental techniques, to unravel and understand the relevant processes for efficient upconversion pumping.

ACKNOWLEDGMENTS

We are grateful to J. R. Quagliano (Los Alamos National Laboratory) who provided and installed the crystal-field programs on our computers. We thank him, M. F. Reid (University of Canterbury, Christchurch), M. P. Hehlen (University of Michigan, Ann Arbor), and H. Weihe (University of Bern) for fruitful discussions. This work has been supported by the Swiss National Science Foundation and the Priority Program Optics of the Board of Swiss Federal Institutes of Technology. Financial support by the Hans-Sigrist Stiftung is gratefully acknowledged.

[1] F. Varsani and G. H. Dieke, J. Chem. Phys. **36**, 2951 (1962).
[2] W. Lenth and R. M. Macfarlane, Opt. Photonics News **3**, 8 (1992).
[3] J. B. Gruber, M. E. Hills, M. D. Seltzer, J. R. Quagliano, M. F. Reid, F. S. Richardson, S. B. Stevens, C. A. Morrison, and T. H. Allik, Phys. Rev. B **48**, 15 561 (1993).
[4] C. K. Jayasankar, M. F. Reid, and F. S. Richardson, J. Less-Common Met. **148**, 289 (1989).
[5] F. S. Richardson, M. F. Reid, J. J. Dallara, and R. D. Smith, J. Chem. Phys. **83**, 3813 (1985).
[6] R. Brede, E. Heumann, J. Koetke, T. Danger, G. Huber, and B. Chai, Appl. Phys. Lett. **63**, 2030 (1993).
[7] A. J. Silversmith, W. Lenth, and R. M. Macfarlane, Appl. Phys. Lett. **51**, 1977 (1987).
[8] M. Takahashi, R. Kanno, and Y. Kawamoto, Mater. Res. Bull. **28**, 557 (1993).
[9] M. P. Hehlen, G. Frei, and H. U. Güdel, Phys. Rev. B **50**, 16 264 (1994).
[10] T. Riedener, K. Krämer, and H. U. Güdel, Inorg. Chem. **34**, 2745 (1995).
[11] K. Krämer and H. U. Güdel, J. Alloys Compd. **207/208**, 128 (1994).
[12] G. Meyer, Adv. Synth. React. Solids **2**, 1 (1994).
[13] W. T. Carnall, G. L. Goodman, K. Rajnak, and R. S. Rana, J. Chem. Phys. **90**, 3443 (1989).
[14] C. A. Morrison, *Angular Momentum Theory Applied to Interactions in Solids* (Springer, Berlin, 1988).
[15] B. R. Judd, J. Chem. Phys. **66**, 3163 (1977).
[16] M. F. Reid, J. Chem. Phys. **87**, 2875 (1987).
[17] C. L. Li and M. F. Reid, Phys. Rev. B **42**, 1903 (1990).
[18] J. R. Quagliano, F. S. Richardson, and M. F. Reid, J. Alloys Compd. **180**, 131 (1992).
[19] J. R. Quagliano, Ph.D. dissertation, University of Virginia, 1993.
[20] M. F. Reid and F. S. Richardson, J. Chem. Phys. **79**, 5735 (1983).
[21] M. F. Reid and F. S. Richardson, J. Phys. Chem. **88**, 3579 (1984).
[22] M. F. Reid, J. Chem. Phys. **87**, 6388 (1987).
[23] M. F. Reid, J. Alloys Compd. **180**, 93 (1992).
[24] D. M. Moran and F. S. Richardson, Phys. Rev. B **42**, 3331 (1990).
[25] D. M. Moran and F. S. Richardson, Inorg. Chem. **31**, 813 (1992).
[26] G. F. Koster, J. O. Dimmock, R. G. Wheeler, and H. Statz, *Properties of the Thirty-Two Point Groups* (MIT Press, Cambridge, MA, 1963).
[27] C. K. Asawa, Phys. Rev. **173**, 869 (1968).
[28] J. C. Eisenstein, J. Chem. Phys. **39**, 2128 (1963).
[29] J. R. Quagliano, N. J. Cockroft, K. E. Gunde, and F. S. Richardson, J. Chem. Phys. **105**, 9812 (1996).
[30] M. P. Hehlen, H. U. Güdel, and J. R. Quagliano, J. Chem. Phys. **101**, 10 303 (1994).
[31] S. R. Lüthi, H. U. Güdel, M. P. Hehlen, and J. R. Quagliano (unpublished).
[32] R. C. Hilborn, Am. J. Phys. **50**, 982 (1982).
[33] G. W. Burdick, C. K. Jayasankar, F. S. Richardson, and M. F. Reid, Phys. Rev. B **50**, 16 309 (1994), and references therein.
[34] P. S. May, C. K. Jayasankar, and F. S. Richardson, Chem. Phys. **138**, 139 (1989), and references therein.